Detection of direct and indirect noise generated by synthetic hot spots in a duct

Francesca De Domenico*, Erwan Rolland, Simone Hochgreb

Cambridge University Engineering Department, Trumpington Street, Cambridge CB2 1PZ, United Kingdom

Abstract

Sound waves in a combustor are generated from fluctuations in the heat release rate (direct noise) or the acceleration of entropy, vorticity or compositional perturbations through nozzles or turbine guide vanes (indirect or entropy noise). These sound waves are transmitted downstream as well as reflected upstream of the acceleration point, contributing to the overall noise emissions, or triggering combustion instabilities. Previous experiments attempted to isolate indirect noise by generating thermoacoustic hot spots electrically and measuring the transmitted acoustic waves, yet there are no measurements on the backward propagating entropy and acoustic waves. This work presents the first measurements which clearly separate the direct and indirect noise contributions to pressure fluctuations upstream of the acceleration point. Synthetic entropy spots are produced by unsteady electrical heating of a grid of thin wires located in a tube. Compression waves (direct noise) are generated from this heating process. The hot spots are then advected with the mean flow and finally accelerated through an orifice plate located at the end of the tube, producing a strong acoustic signature which propagates upstream (indirect noise). The convective time is selected to be longer than the heating pulse length, in order to obtain a clear time separation between direct and indirect noise in the overall pressure trace. The contribution of indirect noise to the overall noise is shown to be non

*Corresponding author
Email address: fd314@cam.ac.uk (Francesca De Domenico*)

negligible either in subsonic or sonic throat conditions. However, the absolute amplitude of direct noise is larger than the corresponding fraction of indirect noise, explaining the difficulty in clearly identifying the two contributions when they are merged. Further, the work shows the importance of using appropriate pressure transducer instrumentation and correcting for the respective transfer functions in order to account for low frequency effects in the determination of pressure fluctuations.

Keywords: Indirect Noise, Entropy Spots, Pressure Transducers

1. Introduction

Acoustic perturbations arising from the heat release in combustion devices are a topic of increasing concern due to stricter noise regulations. The introduction of lean premixed pre-vaporised combustors, which produce low NO_x emissions, but are more sensitive to fuel flow rate and thus pressure fluctuations, has increased noise emissions and the potential for catastrophic instabilities [1]. In the last decade, a significant effort has been undertaken to understand and reduce noise and instabilities whilst maintaining emissions benefits through EU-funded research programmes such as ICLEAC, TIMECOP-AE and RECORD [2, 3, 4]. Pressure perturbations generated in combustors have traditionally been classified into direct and indirect combustion noise. The first is caused by isentropic pressure waves that are produced by the unsteady heat release and propagate towards the turbine [5]. In the second mechanism, local regions of hot gas (hot spots or entropy spots), vortical structures [6] and composition inhomogeneities [7] are produced and then advected toward the turbine with the mean flow. These entropy, vorticity and compositional waves are not directly associated with any pressure fluctuations in the linear regime. However, as they convect through regions with mean flow gradients (such as through turbine vanes or exhaust nozzles) acoustic waves are created, generating indirect combustion noise. These waves travel both upstream into the combustor as well as downstream through the turbine. The upstream-travelling acoustic waves

may couple with the acoustics of the system, stabilising or destabilising the original flame oscillation [8, 9]. Marble and Candel [10] originally developed a one dimensional analytical model, deriving expressions for the magnitude of both direct and indirect noise in the low frequency limit, and more recent work has revisited the issue [8, 9, 11, 12].

One of the main obstacles in the investigation of entropy noise is the lack of unambiguous data linking entropy and pressure fluctuations, owing to the to the complex dynamics of flames in combustion chambers [13]. To overcome this issue, simplified laboratory scale experiments have been designed, in which the flame is replaced with a more easily controlled unsteady source.

Bohn, Zukoski et al. [14, 15, 16] reported some of the first experiments attempting to isolate indirect noise by generating entropy spots synthetically using an electrical heater. However, due to the small temperature increase achieved (1 K) and the poor resolution of the data acquisition system available then, direct and indirect noise could not be separated. This method of generating hot spots was applied more recently in the Entropy Wave Generator (EWG) rig developed at DLR Berlin, to study indirect combustion noise [17, 18]. Acoustic waves resulting from the unsteady electrical heating of thin wires were measured downstream of a convergent-divergent nozzle both in the subsonic and supersonic regime. The DLR experiment generated interest in the community and prompted multiple theoretical and numerical endeavours to explain the experimental results [18, 19, 20, 21, 12, 22, 13]. In the case of the supersonic nozzle the signal was attributed to indirect noise and acoustic reflections [21]. In a study simulating numerically the operation of the EWG under subsonic conditions, Duran *et al.* [12] suggested that the pressure signal obtained was instead mainly due to direct noise. In contrast, according to their model, Lourier *et al.* [22] concluded that direct noise was nearly 6-7 times lower than indirect noise. In all the simulations performed, the acoustic boundary conditions applied had a large influence in the interpretation of the results.

Due to the difficulties in explaining the results of the DLR EWG experiment and the differing interpretations in subsequent analytical and numerical simu-

lations, further experiments have been developed to investigate the phenomena in depth. The Osney Thermo Fluid Laboratory at the University of Oxford has produced an Entropy Wave Generator Test Rig [23] where hot spots are also generated via electrical heating. At Politecnico of Milan a new concept of Entropy Wave Generator has been developed, based on the alternating injection of hot and cold air upstream of a high pressure turbine [24, 25]. Recent experiments have also been performed in the Hot Acoustic Test rig at DLR to investigate the sound generation and propagation due to accelerated cold spots in a nozzle [26].

The aim of all these experiments has been to generate and isolate transmitted entropy noise in a clean and traceable way, without the complications induced by flames or vorticity, so that appropriate models can be suitably validated. To date, there have been no measurements of the upstream entropy noise generated by the acceleration of synthetic hot spots: the experimental data reported so far refers only to the transmitted acoustic waves (acquired downstream of the nozzle). Yet the impact of the backward propagating waves is clear, as they can adversely affect the flame leading to instabilities [8, 9, 27].

The present study aims to investigate the physical mechanisms involved in the generation of direct and indirect noise in a controlled environment. The experiment produces a very simple geometric situation, amenable to one-dimensional modelling. Synthetic hot spots are generated via the Joule effect and accelerated via an orifice plate. The acoustic signal is acquired upstream rather than downstream of the acceleration point; therefore, the results are complementary to other experiments using EWGs.

A detailed description of the experimental apparatus and of the measurement techniques is provided in Section 3. Experimental results for four different configurations are considered, to obtain a comprehensive understanding of the behaviour of the system and provide limit cases for validation of models: (A) an *open end* configuration, with clear boundary conditions; (B) a *closed tube* configuration with no bulk flow, where direct noise can be clearly determined; (C) a set-up where the flow is accelerated in a *subsonic orifice plate*; (D) a set-up

where the flow is accelerated in a *sonic orifice plate*. Direct noise is generated when the heating device is activated, indirect noise when the hot spots are accelerated in the orifice plate, both in subsonic and sonic conditions. The modular set-up enables the unambiguous time separation of direct and indirect noise in the overall pressure trace using a long tube.

Finally, we discuss an important issue which has not been previously reported, regarding the inadvertent use of condenser microphones in the low frequency range typical of entropy spot experiments. In the ultra low frequency range, they behave as a high pass filter, leading to potentially erroneous outputs.

2. Theoretical background

The theoretical underpinnings of the generation of acoustic waves via entropy spots in a flow have been discussed in a number of papers [28, 10], and further developed more recently [9, 12, 29]. Most theoretical studies consider the one dimensional case of hot spots generated from a heating source at rest and then convected through a compact nozzle. A schematic layout of this scenario is represented in Figure 1, where acoustic (P_1^+ and P_0^-) and entropy waves (σ) are generated in an unsteady heat release zone. The heat release zone is considered compact, meaning that its length is much smaller than all the wavelengths considered here (*i.e.* low frequency waves). These waves manifest themselves as fluctuations of pressure p', velocity u' and density ρ' relative to the mean flow pressure, velocity and density ($\bar{p}$, $\bar{u}$, $\bar{\rho}$), and can be represented by their respective amplitudes in the downstream (+) and upstream (-) direction, where (0) and (1) denote the regions upstream and downstream of the heat release interface:

$$P_1^+ \equiv \frac{1}{2}\left(\frac{p'}{\gamma\bar{p}} + \frac{u'}{\bar{c}}\right) \tag{1}$$

$$P_0^- \equiv \frac{1}{2}\left(\frac{p'}{\gamma\bar{p}} - \frac{u'}{\bar{c}}\right) \tag{2}$$

$$\sigma \equiv \frac{p'}{\gamma \bar{p}} - \frac{\rho'}{\bar{\rho}} = \frac{s'}{c_p} \tag{3}$$

If one assumes negligible incoming waves ($P_1^- = P_0^+ = 0$), one can derive expressions for the amplitudes of the waves generated at the heat release zone from the conservation of mass, enthalpy and entropy [12]:

$$P_1^+ = \frac{1}{2}\left(\frac{\overline{M}}{1+\overline{M}}\right)q' \tag{4}$$

$$P_0^- = \frac{1}{2}\left(\frac{\overline{M}}{1-\overline{M}}\right)q' \tag{5}$$

$$\sigma = q' \tag{6}$$

where $\overline{M}$ is the mean Mach number and q' is the non-dimensionalised value of the fluctuating heat release $\dot{Q}'$ ($q' = \dot{Q}'/\dot{m}C_p\bar{T}$). These acoustic waves are referred to as 'direct' noise, as they are a direct result of the unsteady heat release. The acoustic waves thus generated propagate at the speed of sound $\bar{c}$ relative to the mean flow, and are reflected at the inlet and outlet of the duct having acoustic reflection coefficients $R_{i,a}$ and $R_{o,a}$, respectively (Figure 1).

The entropy spots are advected downstream with the mean flow without generating an acoustic signature in the linear approximation [28]. If these waves are accelerated, they generate sound waves which propagate both downstream and upstream of the outlet. Marble and Candel [10] derived expressions for the amplitude of a single backward-propagating (or 'reflected') wave due the acceleration of an hot spot for a compact nozzle (P_s^-) under subcritical and supercritical (choked) isentropic conditions, between two sections with Mach numbers M_1 and M_2, respectively:

$$P_s^- = -\frac{M_2 - M_1}{1 - M_1}\frac{\frac{1}{2}M_1}{1 + \frac{1}{2}(\gamma-1)M_1M_2}\sigma \tag{7}$$

Under critical conditions, we have $M_2 = 1$, so that:

$$P_s^{-*} = -\frac{1}{2}\frac{M_1}{1 + \frac{1}{2}(\gamma-1)M_1}\sigma \tag{8}$$

The acoustic waves generated in this manner are referred to as 'indirect' noise, as they are only indirectly related to the unsteady heat release upstream. In this paper, the terms 'indirect noise' and 'entropy noise' are used interchangeably to indicate acoustic waves generated from the acceleration of entropy spots both upstream and downstream of the nozzle. From Marble and Candel [10], the reflected indirect noise is a negative perturbation relative to the mean, whereas the direct noise resulting from a single perturbation of the heat release q' is positive as shown in Eq. 4 and 5 and further on in the experimental results. In the absence of acoustic reflections at the boundaries, in an idealised one dimensional situation, the shape of the direct and indirect acoustic waves in the time domain is expected to be identical to that of the heat fluctuation q' at the heating grid and at the nozzle respectively (*e.g.* a square heat pulse should lead to a square acoustic pulse). Dispersive effects owing to molecular or turbulent diffusion alter the original shape of the non-uniformity, thus affecting the final pressure perturbation [30].

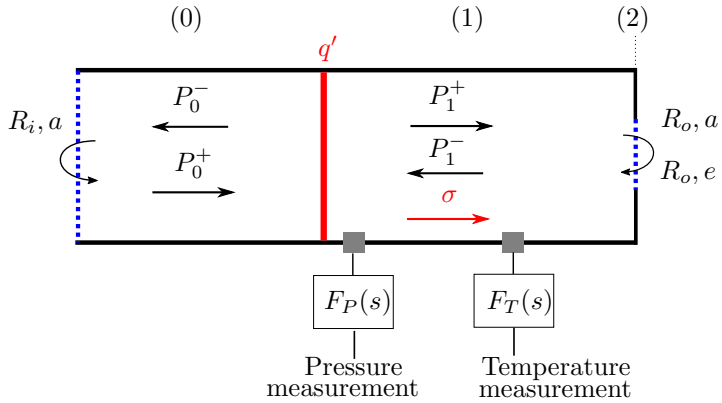

Figure 1: Experimental layout including pressure transducer transfer function $F_P(s)$ and thermocouple transfer function $F_T(s)$.

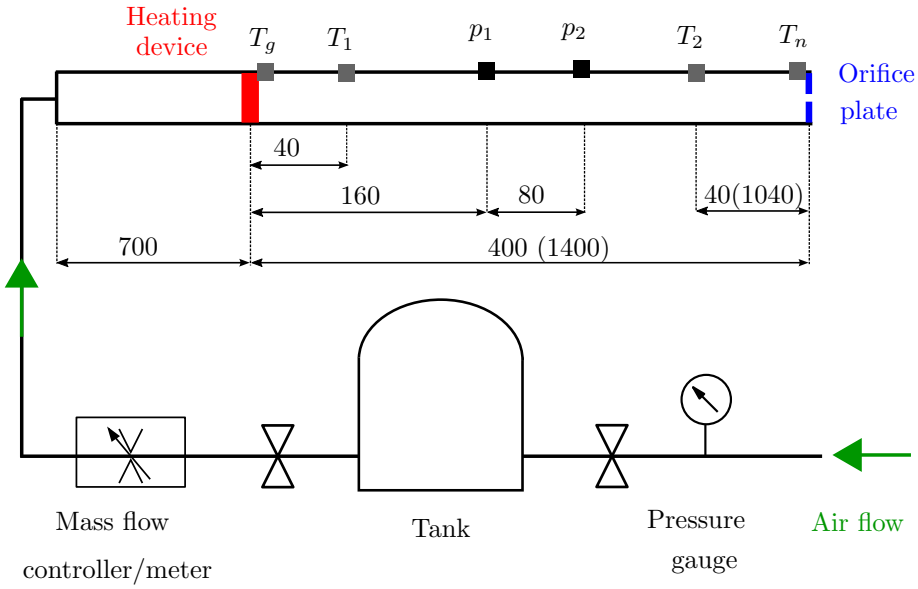

Figure 2: Schematic of the experimental set-up (values in parentheses correspond to the long tube configuration). Dimensions in mm. Dimensions not to scale.

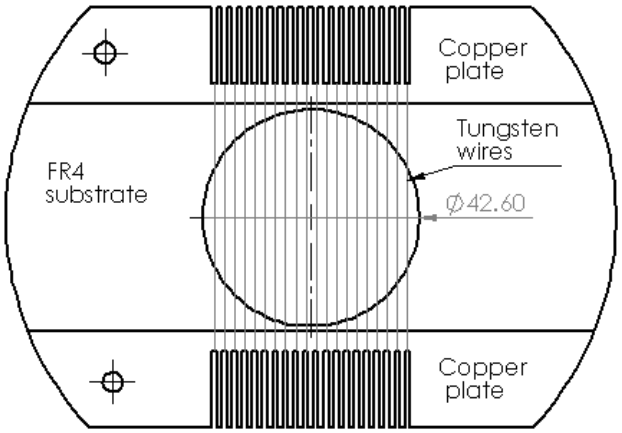

Figure 3: Schematic of the heating grid. Dimensions in mm

3. Experiment

3.1. Instrumentation

The experimental set-up is shown in Figure 2. Air flows through a tube at a controlled rate. Hot spots are produced synthetically by pulsing current through a heating device, generating a heat release pulse via the Joule effect. The air flow exits through an orifice plate, which can be operated in subsonic and sonic conditions. The hot spots are convected with the flow, and generate indirect noise as they accelerate through the orifice. Dynamic temperature and pressure measurements are performed downstream of the heating device, via flush-mounted pressure transducers or thermocouples, as described further on.

Filtered compressed air from the laboratory air supply system is fed into a 250 L tank to dampen out upstream pressure oscillations. The tank pressure is set to 5 bar using a pressure gauge. The tank is connected via a 12 mm inner diameter plastic hose to a mass flow controller (MFC, Alicat MCR250, accuracy, $\pm$ 1% full scale), or a mass flow meter for high flow rates (MFM, Alicat MCR3000, accuracy $\pm$ 1% full scale). The MFC/MFM are connected to the test section via a 12 mm, 1.2 meter long plastic hose via a flat flange to provide a simple boundary condition.

The tube has an inner diameter of 42.6 mm and is made from sections of PVC and stainless steel 316. The PVC tube inner diameter is slightly larger than the steel tube by 0.2%, so the discrepancy is assumed to be negligible. The different materials are used to address both safety and sealing considerations: the PVC pipe is lighter and easier to handle, but is prone to air leakages if fitted with transducer ports. Thus, it is used only in the sections of the tube where there are no transducers.

The heating device (Fig. 3) is fitted 700 mm downstream of the tube inlet via a PVC flange for electric isolation. The device itself is composed of three grids of thin tungsten wires (58 μm diameter) connected in series, with an overall resistance of about 1 Ω. Each grid is made of 2.3 m of wire wound around a FR4 substrate 1.6 mm thick, which keeps the wires in place using a

toothed comb structure. Two copper plates connect the wires on both faces of the module, so that each heating grid is electrically equivalent to 42 parallel 45-mm-long resistances of tungsten wire. Two consecutive grids are separated by a FR4 insulating plate 1.6 mm thick. The heating device is roughly 10 mm thick, and therefore it can be approximated as a compact element for low frequency disturbances. An in-house circuit controlled by a computer drives a power supply (Glassman Lp 60-20), and delivers a current pulse of 21 A to the heating device, with a duration set to 200 ms for all experiments.

The experimental set-up is flexible, and can be operated in several configurations to cover a large range of operating conditions. The length of the tube downstream of the heating device can be varied to modify the convective distance travelled by the hot spots before being accelerated. In the short tube configuration, this distance is 400 mm, whereas in the long tube case, it is 1400 mm. These two different tube lengths have been chosen to enable a partial-total time separation between the generation of the heating pulse and the acceleration of the hot spots. In this way, direct and indirect noise can be initially separated in time and afterwards partially merged in time.

Two orifice plates are used: one with a 6.6 mm diameter hole (8 mm thickness), and a second with a 3 mm diameter hole (5 mm thickness). An orifice plate is easier and cheaper to manufacture than a convergent nozzle but the two are expected to behave in the same way regarding both the direct and the indirect noise generated. In a first approximation, the flow through a generic area decrease interface can be assumed to be isentropic [31]. Additionally, both the orifice and the nozzle are expected to behave as a compact sources in the frequency range of the experiment.

The air temperature is determined using thin K-type thermocouples (fine gauge exposed welded tip thermocouples type K, 0.076 mm wire diameter, labelled T_i in Figure 2), whose time constant is found experimentally to be around 300 ms. In order to correct for the long response time relatively to the 200 ms heating pulses, a hot film anemometer (Dantec gold plated wire probe type 55R01) with a wire diameter of 5 μm (response time under 10^{-4} ms) is used to

obtain the shape of the temperature pulse. The pressure signal is acquired with condenser microphones and piezoresistive pressure transducers at the locations P_i: two G.R.A.S. 40bp (IEC 61094 WS3P 1/4") externally polarised condenser microphones connected to the G.R.A.S. 26AC 1/4" standard preamplifier, two Kulite XTE-190(M) piezoresistive pressure transducers and a Kulite XT-140M piezoresistive absolute pressure transducer. The transducers are either placed on the same axial plane for calibration cross checking, or along the tube at stations downstream of the heating module. The outputs of the piezoresistive pressure transducers are amplified with a Fylde FE-379-TA modular DC amplifier. Both the Kulite and G.R.A.S. transducers are connected to a NI PCI-5259 board via a NI-2090 DAQ box. The sampling rate used is 8192 samples per second, with a 16-bit resolution.

3.2. Flow rate measurements and conditions at the throat

The flow meter/controller records the volumetric flow rate (Q), mass flow rate ($\dot{m}$), temperature T_f and pressure at the flowmeter P_f at a sampling rate of 20-30 Hz. The bulk flow velocity $\bar{U}$ is calculated as:

$$\bar{U} = \frac{\dot{m}}{A\bar{P}/R\bar{T}} \tag{9}$$

where A is the inner cross-sectional area of the tube, $\bar{P}$ and $\bar{T}$ are the measured pressure and temperature in the tube and R is the gas constant for air. In the present analysis, the mean temperature in the tube $\bar{T}$ is assumed to be identical to that acquired at the flow meter T_f since the difference between these two temperatures is expected to be lower than 1%.

The Mach number at the orifice plate throat is necessary to estimate the intensity of the entropy noise, yet it is difficult to measure it directly in subsonic conditions. A calculated value for the Mach number M_T at the throat can be obtained by assuming isentropic expansion from the measured mean pressure in the straight section of the tube, $\bar{P}$, to the pressure at the throat, estimated to be atmospheric pressure ($P_T = P_a$).

$$M_T^2 = \frac{2}{\gamma - 1}\left[\left(\frac{\bar{P}}{P_a}\right)^{\frac{\gamma-1}{\gamma}}\left(1 + \frac{\gamma-1}{2}\bar{M}^2\right) - 1\right] \tag{10}$$

The upstream pressure $\bar{P}$ is measured using the Kulite absolute pressure transducer, and the upstream Mach number $\bar{M}$ is calculated from the bulk velocity and mean temperature ($\bar{M} = \bar{U}/\sqrt{\gamma R\bar{T}}$).

The markers in Fig. 4(a) show the upstream pressure $\bar{P}$ and velocity $\bar{U}$ measured in the tube at several operating points for the 3 mm (red dots) and 6.6 mm (black triangles) orifice. The lines represent the theoretical relation between upstream pressure and velocity assuming an ideal isentropic convergent nozzle with a vena contracta factor $\Gamma = 1$. Figure 4(b) shows the calculated nozzle Mach number (obtained from Eq. 10) versus the upstream bulk flow velocity, comparing the experimental results with the theoretical predictions for an ideal isentropic convergent nozzle. The discrepancy between the ideal and measured cases are due to the vena contracta factor of the orifice which is around 0.8 for all cases.

3.3. Characteristics of the heating pulse

Figure 5 shows the normalised current signal pulsed into the heating module and the induced temperature increase in the flow, detected with the anemometer 0.5 m downstream of the grid. The current signal is normalised to the maximum nominal current delivered from the power supply, 21 A. In all experiments the current is set to its maximum limit (I_{max}), while the voltage is set to 35 V. The heating module has a resistance $R \sim 1\ \Omega$, requiring a voltage $V = RI_{max} = 21$ V, and the excess energy is dissipated. However, in the first few milliseconds of the pulse, the capacitor in the driving system leads the power supply to release a higher current, before it auto-adjusts the current to its maximum nominal limit. The initial peak in the delivered current makes the wires warm up faster than they would do with a square pulse. It can be observed that there is no relevant time delay associated to the electric circuit: the time constant of the RC circuit is much shorter than the characteristic times of the experiment.

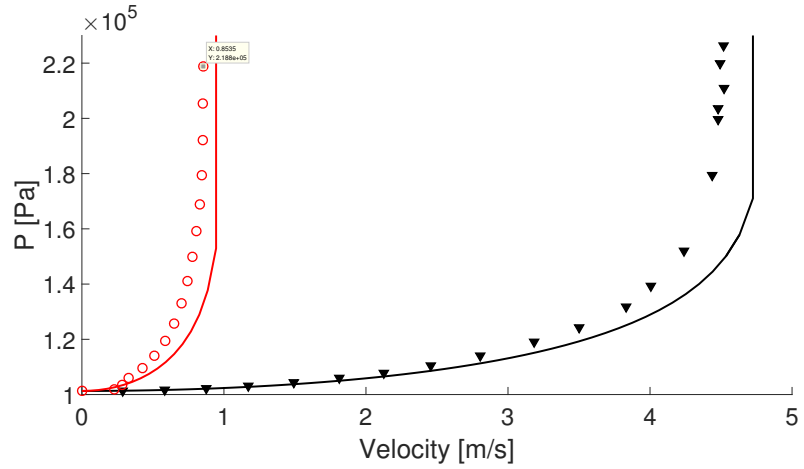

(a)

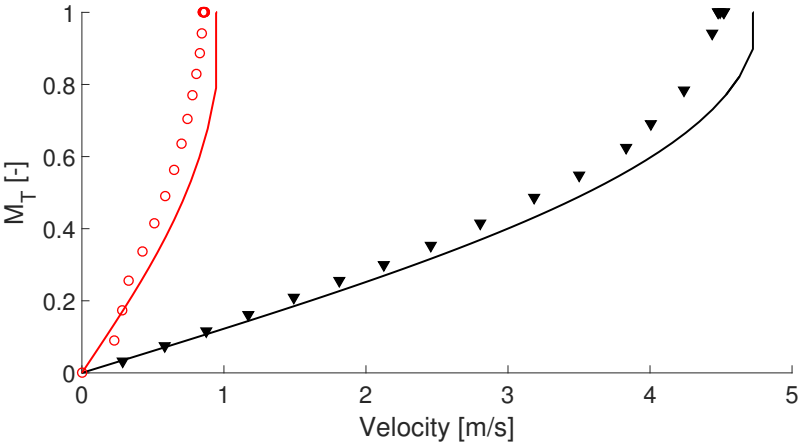

(b)

Figure 4: Calculated upstream pressure (a) and nozzle Mach number (b), as a function of bulk flow velocity for the 3.0 mm (red circles) and 6.6 mm (black triangles) diameter orifices. Lines represent the corresponding isentropic values with $\Gamma = 1$.

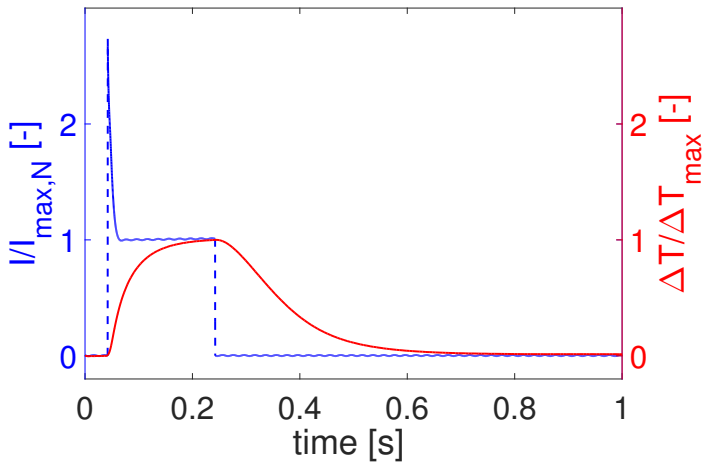

Figure 5: Current pulse delivered by the driving system into the heating module normalised by the maximum nominal current of the power supply $I_{max,N} = 21$ A (blue dashed line); temperature rise profile of the hot spot signal acquired in the centre of the tube by the anemometer normalised by the peak temperature T_{max} (red solid line).

3.4. Temperature measurements

Accurate information regarding the temperature and shape of the hot spots generated by the heating device is crucial to understand and model the experiment. Three pieces of information are particularly important: the shape of the response of the temperature pulse in the time domain, the maximum temperature change induced in the air flow, and finally the spatial behaviour of the hot spots (how they spread and disperse before reaching the orifice). The transient nature of the heating process makes obtaining accurate measurements challenging. In order to overcome these difficulties, both thermocouple and hot film anemometry measurements are performed simultaneously. Thermocouples are often used to determine a gas temperature, but, due to the inertia of the thermal junction, their transient output is slower-rising with respect to the actual input signal. For a given temperature input $T_I(s)$, they produce an output $T_O(s)$

$$T_O(s) = \frac{1}{1 + s\tau_{tc}} T_I(s) \tag{11}$$

where τ_{tc} is the time constant of the thermocouple.

Figure 6 shows how the actual temperature increase at a given location in the tube (in this case, just downstream of the heating grid) is reconstructed (red dotted line). Commercial beaded wire thermocouples with small diameters (0.076 mm) are used to obtain measurements of the asymptotic temperature rise. For these thermocouples an average time response $\tau_{tc} = 300$ ms was experimentally determined with a step input and an air flow of 20 m/s. For lower flow velocities, the time constant is higher. Therefore, in the 200 ms of the pulse, the thermocouple displays a slower-rising and attenuated output (dashed lines in figure 6) with respect to the temperature input.

From the temperature signal in Fig. 5 it can be noted that in 200 ms the hot spot temperature nearly saturates, which suggests that the wires of the grid have reached their maximum temperature. If the same current and voltage are pulsed into the grid for a time t_p sufficiently long ($t_p > 3\tau_{tc}$) the thermocouples have enough time to asyntothise and acquire the actual value of the temperature. Therefore, the peak temperature value displayed after the 1.5 s long pulses (dashed-dotted lines in Fig. 6) is a good representative of the actual peak temperature of the hot spot. The shape of the temperature pulse is reconstructed more precisely using a hot film anemometer (dotted line in Fig. 6). The 5 μm Dantec probe has a negligible response time compared to the pulse duration. For moderate variations of the air temperature T_a ($\Delta T_a \sim$ 10-80 K), assuming negligible variations in the bulk flow velocity, the output voltage variation ΔE can be expressed as [32]:

$$\Delta T_a = -2\frac{T_W - T_{a,0}}{E_0}\Delta E \approx -\beta \Delta E \tag{12}$$

where T_W is the temperature of the hot wire ($T_W \sim$330°C). For small temperature increases, the change in the output voltage of the anemometer is in a first approximation proportional to the change in the air temperature. Assuming that the anemometer captures the shape of the temperature pulse without distortion or attenuation, the shape of the output voltage of the anemometer is

used to represent of the shape of the hot spot.

The different measurements of the air temperature are kept as consistently as possible, but there is an estimated uncertainty of ±2 K in the determination of the absolute value of the air temperature rise. This is due to: (i) difficulties in accessing the correct location for some measurements (*i.e.* as close as possible to the heating grid and to the nozzle), (ii) internal differences between the transducers, and (iii) small and uncontrollable variability of the test conditions (*e.g.* replacement of the heating module). The tests for acquiring the air temperature at the grid are performed with an open tube, to enable the thermocouple to be placed as close as possible to the heating grid. It is assumed that the same heating power delivered to the same mass flow rate leads to the same temperature increase in an open and closed tube configurations.

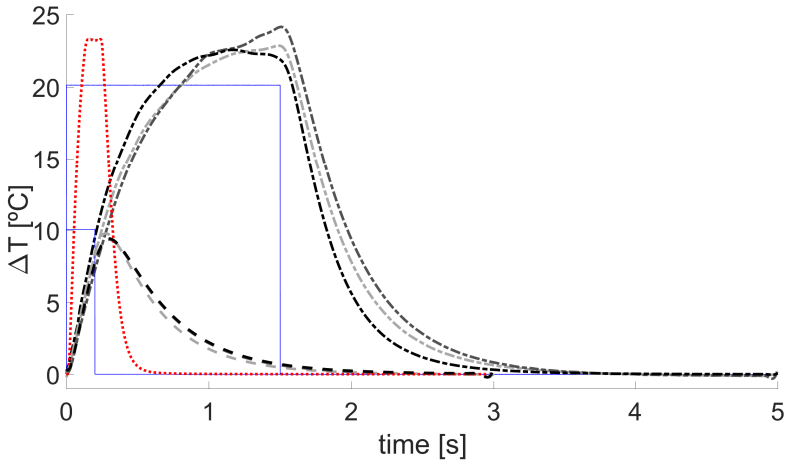

Figure 6: Temperature profiles acquired with three nominally identical thermocouples downstream of the heating grid, mean flow velocity of 1 m/s for a 200 ms pulse (dashed lines) and a 1.5 s pulse (dashed-dotted lines). Solid lines: short and long input pulses. Anemometer output (red dotted line) normalised using the measured temperature rise.

3.5. Pressure transducer characteristics

Piezoresistive pressure transducers and microphones convert an acoustic signal into an electrical signal. Piezoresistive transducers rely on the piezoresistive effect that occurs when the electrical resistance of a material changes in response to applied mechanical strain [33]. They offer a flat frequency response and zero phase shift even at very low frequencies. Microphones translate pressure fluctuations into a voltage via a diaphragm or a cantilever beam exposed to the incident sound pressure, using cavities and vents as pressure equalisation channels. Microphones therefore act as differential pressure measurements with capacitance, so that the sensors only respond to dynamic pressure fluctuations, unlike pressure transducers [34, 35]. The added capacitance means that at low frequency they behave as a high pass filter, with lower gain and shift in phase. On the other end, capacitive microphones are capable of higher sensitivity and dynamic range than piezoresistive pressure transducers.

The transfer function $F_p(f)$ of a condenser microphone such as the G.R.A.S. 40bp has been shown to be well represented by that of a high pass filter function [33, 34]:

$$F_p(f) = G\frac{i\frac{f}{f_0}}{1+i\frac{f}{f_0}} \tag{13}$$

where f_0 is the cut-on frequency of the microphone and G is the frequency-independent sensitivity of the microphone, called open-circuit voltage [33]. In the present experiment we calibrate the response of the condenser microphone to show that its corrected response can yield the original pressure data.

3.5.1. Predicted and measured transfer function of G.R.A.S. microphones

The high pass filter behaviour of the two G.R.A.S. condenser microphones was measured at frequencies from 1 to 40 Hz, using a calibrated Kulite transducer as a reference, as its output is not distorted at low frequencies. The test tube is attached to a plenum by means of a conical intake, where two opposed loudspeakers are housed. The two loudspeakers excite the tube by generating sinusoidal acoustic waves at a given frequency. All of the transducers are located

on the same axial plane along the tube, exposing them to the same pressure signal in the plane wave approximation.

The differences in gain and phase between the signals acquired by the two G.R.A.S. microphones and the Kulite reference transducer are shown in Figure 7. As expected, the signals displayed by the G.R.A.S. transducers are attenuated (Fig. 7(a)) and phase shifted (Fig. 7(b)). The two G.R.A.S. transducers behave slightly differently at low frequencies. The cut-on frequency was experimentally determined as 1.02 Hz, with a phase shift of $\pi/4$. This is consistent with the G.R.A.S. 26AC 1/4" standard preamplifier specifications, according to which the cut-on frequency of typical 1/4" microphones is around 1 Hz, as measured [36]. Indeed, from the specifications in the datasheet, the G.R.A.S. 40bp microphones have a frequency range ($\pm$2 dB) of 4 Hz to 70 kHz.

3.5.2. Experimental demonstration of the signal distortion for capacitive microphones

Prior to introducing tests with the heating device, low frequency pulsed excitation using a cold air pulse is used to test the G.R.A.S. sensor response relative to the Kulites, both with and without the microphone transfer function. Pulsating mass flow is injected by driving the mass flow controller with square pulses at 0.22 Hz frequency and a duty cycle of 15%. The mass flow controller valve rise time is only 7.4 ms according to the specifications. Measurements are carried out over a period of 32 seconds with a sampling frequency of 2048 Hz. Due to the presence of the orifice plate at the end of the tube, an increase in the flow rate leads to a pressure increase in the tube. Indeed, from Figure 8, it can be seen that the Kulite pressure transducers display the expected shape of the outputs in the form of a pressure rise to a final value (black solid line), whereas the raw signal of the G.R.A.S. transducers (red dashed line) produces a smaller rise and a ringing negative pulse at this low frequency. The red dashed-dotted line shows the output from the G.R.A.S. sensors when corrected by the corresponding transfer function in Eq. 13 using the experimental values for f_0. An adequate match in shapes and amplitudes with the Kulite transducers is

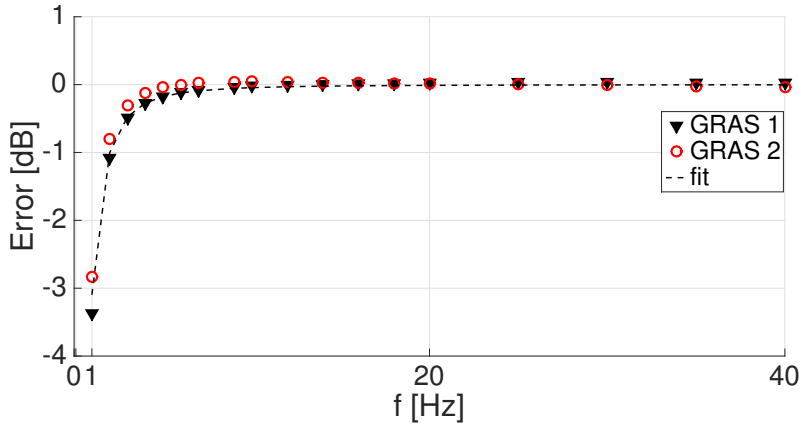

(a)

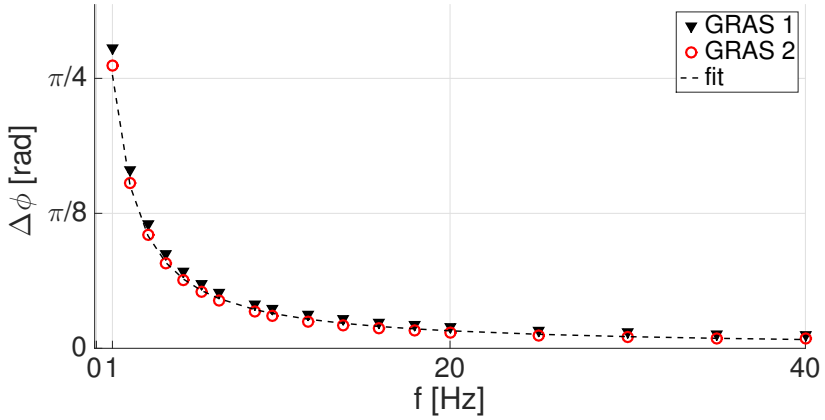

(b)

Figure 7: Difference in gain (a) and phase (b) between signals from the reference Kulite and G.R.A.S. transducers (markers), along with the differences for the best fit high pass filter transfer function (dashed line) obtained from the experimental data.

obtained.

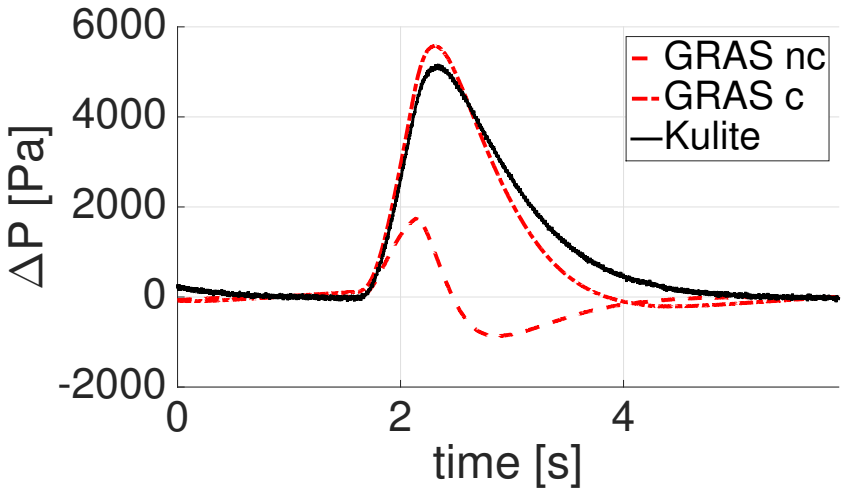

Figure 8: Pressure profile acquired after pulsating mass injection in the tube from Kulite (black solid line) and G.R.A.S. (red lines) transducers. G.R.A.S. microphone raw signal (dashed line) and corrected by the transfer function (dashed-dotted line).

4. Results

The response of the system to the generation and convection of synthetic hot spots was measured for four cases: (A) *open tube with flow*, the tube is terminated with an open end; (B) *closed tube with no flow*, the tube is terminated with a rigid cap; (C) *accelerated flow (subsonic)*, the tube is terminated with the 6.6 mm hole orifice plate; (D) *accelerated flow (sonic)*, the tube is terminated with the 3.0 mm hole orifice plate, which is choked. These cases are summarised in Table 1. The four cases are used to obtain a clearer understanding of the behaviour of the system and provide a comprehensive frame for further modelling. Indirect noise can be generated only in cases (C) and (D), where the hot spots are accelerated in the orifice. The open and closed cases (A and B) add limit situations for comparison and provide information useful to identify the acoustic properties of the system, such as dissipative effects and

reflection coefficients at the boundaries. In to the ultra-low frequency range of the experiment, traditional techniques for impedance measurements, such as multi microphone methods, cannot be easily used [37]; the present experiments allow the reflection coefficients and the system physics to be extracted from the resulting signal in the open and closed cases as references.

The pressure signals shown in this section are acquired 160 mm downstream of the heating module. All the experiments are carried out in the long tube configuration (1400 mm convective length downstream of the heating module) and the short tube configuration (400 mm convective length). A current of 21 A is pulsed for 200 ms with a voltage of 35 V; both the power and the energy are kept constant for all tests. The pulse period is set to 3 s to obtain a clear time separation between the acoustic oscillations caused by successive pulses. The air flow in the tube is varied between 78 and 250 slpm. The acquisition time is set to 512 seconds, so that the signals are averaged over 170 pulses. Within one test, the normalised RMS deviation on the acquired temperature measurements (calculated on the peak temperature values) is around 2%.

The mean air flow temperature measured at the flowmeter varies between 19 and 21°C depending on the environmental conditions, and it is taken as 20°C on average. The data is filtered with a 0-100 Hz rectangular window digital filter.

Case	Description	Tube termination
A	Open tube with flow	Open tube
B	Closed tube without flow	Rigid wall
C	Accelerated flow (subsonic)	Orifice (6.6 mm)
D	Accelerated flow (sonic)	Orifice (3.0 mm)

Table 1: Overview of the four experimental cases

4.1. Case A: Open tube

Figures 9 show pressure signal results for Case A (open-ended tube) with a mean flow velocity $\bar{U}$= 2.27 m/s (upstream Mach number = 0.0066), in the long

(a) and short (b) tube configurations. The acoustic pressure signal measured in the tube is very low, with a few peaks due to the initial gas expansion during heating. The theoretical reflection coefficient of an open end $R_{o,a}$ is close to -1 in the low frequency range, meaning that the forward propagating acoustic waves generated by the heating device (direct noise) are approximately instantaneously reflected with an opposite sign at the outlet and propagate back into the tube. The forward and backward waves in the tube nearly cancel out, explaining why the pressure in the tube oscillates around zero. In the long tube data (Fig. 9a), the oscillation frequency $f \simeq 38$ Hz corresponds to a quarter of wave modes ($\lambda/4 \simeq L$), which is consistent with the fact that the inlet of the tube behaves as a closed wall ($R_{i,a} \simeq +1$).

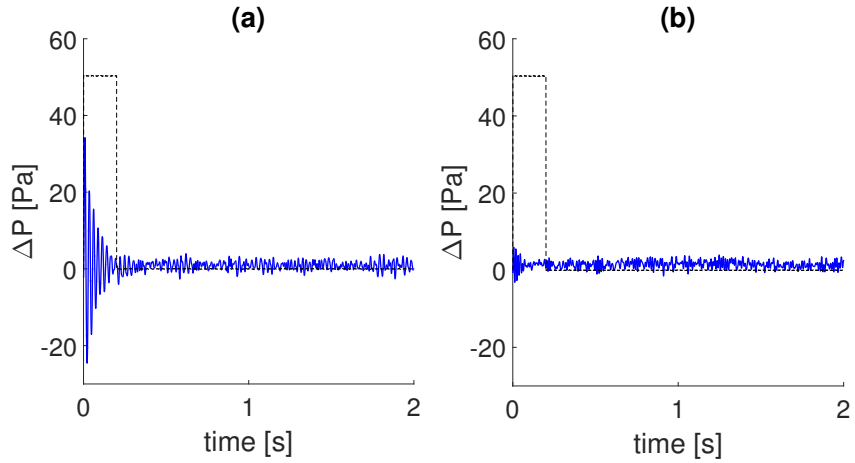

Figure 9: Ensemble-averaged pressure signals as a function of time obtained with an upstream Mach number M=0.0066 and open tube in the short (a) and long (b) tube configuration.

4.2. Case B: Closed tube

Figure 10 shows the results for Case B (closed tube) with no mean flow. When the heating device is active, the adjacent fluid is heated by conduction (the air trapped inside the tube is still) and tends to expand. The sudden expansion of the fluid, constrained by the inertia of the unperturbed media, acts as a piston on the rest of the gas, creating a local pressure disturbance which leads to the

generation of acoustic waves that propagate along the tube at the speed of sound (thermoacoustic convection) [38, 39, 40, 41]. The acoustic waves generated from the heat source impinge on the walls, and are reflected back with the same sign as the original wave (the theoretical reflection coefficient at the rigid walls $R_{i,a}$, $R_{o,a}$ is 1). Subsequently, these waves repeatedly traverse between the boundaries. Given that the acoustic time-scale is an order of magnitude smaller than the pulse duration, these acoustic waves are essentially accumulating while the heating device is active. Once the heating device is switched off, the acoustic energy decays due to losses at the boundaries and viscous and thermal losses within the fluid.

For the short tube (black solid line) the maximum pressure is higher and the pressure rises faster than for the long tube (red dashed-dotted line). Indeed, the tube boundaries are closer together, meaning that the acoustic round trip time is shorter, and the acoustic waves are reflected more times during a given interval than in the long tube configuration. As a result, the acoustic pressure build up in the shorter tube is faster, leading to a higher maximum pressure.

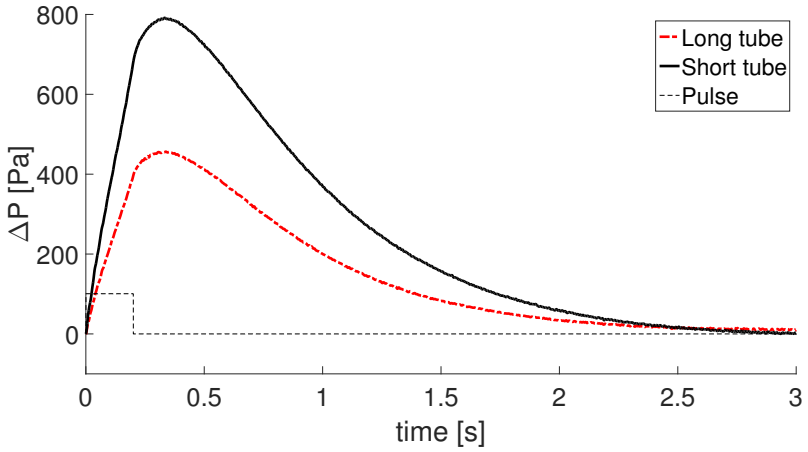

Figure 10: Ensemble-averaged pressure signals obtained after the heating pulse with closed boundaries (rigid wall at the end) for the short (black solid line) and long (red dashed-dotted line) tube configuration.

4.3. Case C: Accelerated flow (subsonic)

In these experiments, the downstream end of the tube is terminated by the 6.6 mm orifice plate, through which the air flow accelerates. The experimental conditions tested are listed in Table 2. It was experimentally determined that the bulk flow velocity required to choke the flow with the 6.6 mm orifice is 4.2 m/s (see Figure 4 in Sec. 3.2) therefore the flow through the orifice is subsonic in the test conditions listed.

	$\bar{P}$ $[kPa]$	$\bar{U}$ [m/s]	M_T	ΔT_g $[K]$	ΔT_S $[K]$	ΔT_L $[K]$
1	102.78	0.88	0.1441	26.7	19.1	7.9
2	103.54	1.12	0.1771	21.1	16.1	8.2
3	104.00	1.24	0.1942	19.5	15.1	8.0
4	105.19	1.49	0.2327	15.9	12.5	7.5
5	106.64	1.75	0.2719	13.3	10.9	6.8
6	108.34	1.98	0.3114	11.7	9.9	6.1
7	110.86	2.27	0.3613	10.5	8.5	5.9
8	113.65	2.56	0.4088	9.2	7.6	5.7

Table 2: Operating conditions for Case C (accelerated subsonic flow) for the long tube (1.4 m convective length downstream of the heating module) and the short tube (0.4 m convective length). $\bar{P}$: mean pressure at the grid; $\bar{U}$: bulk flow velocity at the grid; M_T: estimated Mach Number at the throat (see Sec. 3.2); ΔT_g: measured peak temperature rise of the hot spots at the grid; ΔT_S: measured peak temperature of the hot spots 0.4 m downstream of the heating module (location of the orifice plate for the short tube); ΔT_L: measured peak temperature of the hot spots 1.4 m downstream of the heating module (location of the orifice plate for the long tube)

4.3.1. ***Long tube***

Figure 11 shows the pressure signal obtained 160 mm downstream of the heating module in the long tube configuration. The velocity of the flow is kept low in order to obtain a clear time separation between the heating pulse and the time at which the hot spots arrive at the outlet. Since all the tests are performed by pulsing the heating device at a constant power, increasing

the volumetric (and mass) air flow through the heating device decreases the measured temperature rise induced in the flow, as can be seen in Table 2. Two thermocouples are located in the orifice to detect the arrival of hot spots at the outlet of the tube. Figure 12 zooms on Case C-3 (Table 2) to identify the characteristic components of the acoustic signal.

The air temperature time history in figure 12 is reconstructed from the output of the thermocouple and the anemometer using the method described in Sec. 3.4. The data are recorded at three different positions (L_c) downstream of the heating grid: 0.05 m, 0.4 m (end of the short tube) and 1.4 m (end of the long tube). It is assumed that the temperature signal 0.05 m from the heating grid well approximates the temperature signal at the grid. The shape of the temperature signal close to the heating grid has a higher and sharper peak, whilst for longer distances the hot spot spreads out and the temperature signal is more disperse.

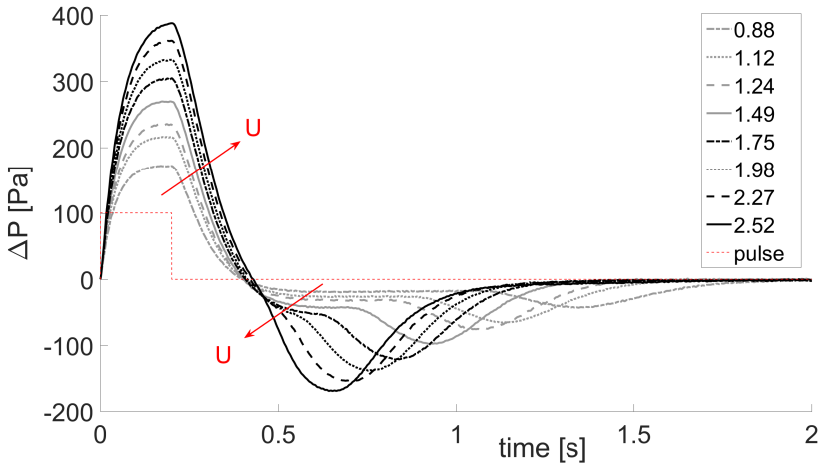

Figure 11: Ensemble-averaged pressure signal acquired by the Kulite transducer 160 mm downstream of the heating module for the cases listed in Table 2 (long tube). Legend indicates the magnitude of the bulk velocity (U) in m/s.

From Figure 12 a strong acoustic signal is observed in the tube while the heating device is active: there is a negligible time lag between the driving pulse and the observed pressure pulse. For a distance $L_p = 0.16$ m between the

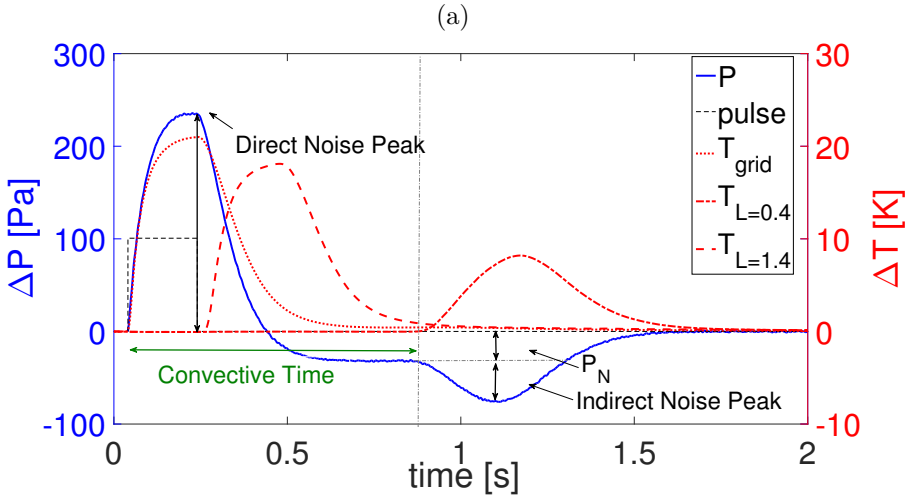

Figure 12: Detail of operating condition C-3 ($\bar{U}$ = 1.24 m/s): identification of direct noise, indirect noise, convective time on the pressure trace (solid blue line); and reconstructed air temperature profile acquired at three different convective lengths (L, in m) downstream of the heating module (respectively dotted red line for L = 0 m, dashed red line for L =0.4 m and dashed-dotted red line for L =1.4 m).

heating grid and the pressure acquisition point, this time lag is $\tau_p = L_p/c \sim 5 \times 10^{-4}$ s, which is of the order of the time resolution of the acquisition system ($\tau_S = 1/8192 \sim 1.2 \times 10^{-4}$ s). In all 8 cases, the pressure reaches a positive maximum at the end of the heating pulse. Therefore, it can be concluded that these positive pressure rises represent the direct noise. When the hot spots arrive at the orifice and are accelerated through it (as detected by the thermocouple signal), smaller negative excursions are observed. As the flow velocity increases (and the convective time decreases), these negative dips occur earlier in time. Therefore, these negative peaks are attributed to the acceleration of hot spots through the orifice plate, the so-called indirect noise. A third contribution to the acoustic signal can be seen in the pressure signal in Figure 12: after the direct noise peak, the pressure fluctuation does not return to zero, but becomes negative (negative oscillation labelled P_N). This effect may arise from the mean lower density of the flow, but requires further investigation.

Figure 13(a) shows the peak values of the direct and indirect noise against the estimated orifice Mach number. The indirect noise peak is evaluated by subtracting P_N from the minimum value of the pressure trace as shown in Figure 12(a). Both direct and indirect noise peaks increase approximately linearly as the Mach number is increased. However, the amplitude of the direct noise is nearly four times larger than that of the indirect noise. Figure 13(a) shows that under subsonic conditions the effect of indirect noise is not negligible. Even at small Mach numbers at the orifice (*i.e.* low accelerations), and for small temperature fluctuations, there is still a clear sign of indirect noise, in contrast to the findings for subsonic conditions in previous experiments [12, 26]. In Figure 13(b), the maximum absolute values of direct and indirect noise from Figure 13(a) are normalised by the corresponding peak temperature increase of the air at the grid and at the nozzle (values reported in Table 1), and non-dimensionalised by the mean pressure and temperature in the tube. Both the normalised direct and indirect noise are directly proportional to the nozzle Mach number. Considering that the peak temperature at the nozzle is lower than the peak temperature at the heating grid, the normalised indirect noise becomes comparable to the normalised direct noise. However, for higher velocities, the ratio of the hot spot temperature at the nozzle and at the grid becomes smaller, which explains the different slopes of the two curves. This shows that in this experiment the direct noise has a significant influence and cannot be neglected.

The direct noise caused by the heating of the wires always reaches its maximum at the end of the heating pulse ($t = 200$ ms). As the flow rate (and the velocity) increases, the time separation between the direct and the indirect noise peaks becomes shorter, due to the decrease in the convective time. These results suggest an important issue in the identification of indirect noise: increasing the flow velocity can increase the relative contribution of indirect noise through higher acceleration in the nozzle, yet the convective time of hot spots decreases. When the convective time becomes similar to the pulse length, direct and indirect noise start merging, and a clear time separation between the two is no longer possible. However, because the direct noise is typically higher (Figure

13), the effect of the indirect noise can not be distinguished in a straightforward way: if the merging effect is not considered, it can be erroneously concluded that there is no indirect noise in the system.

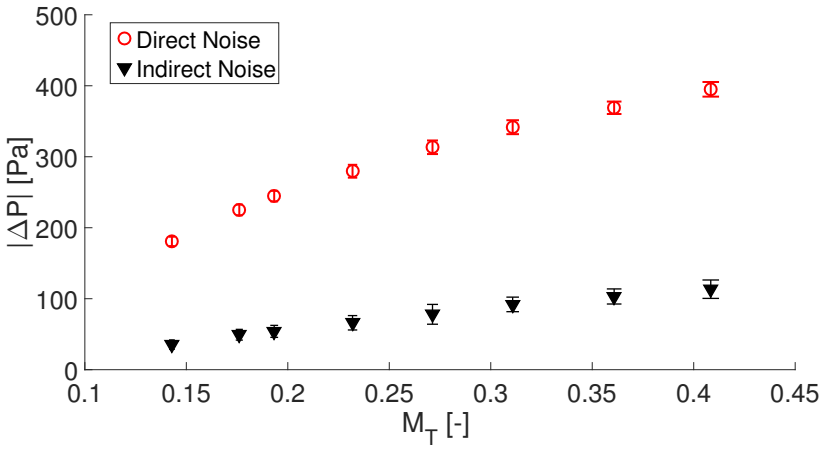

(a)

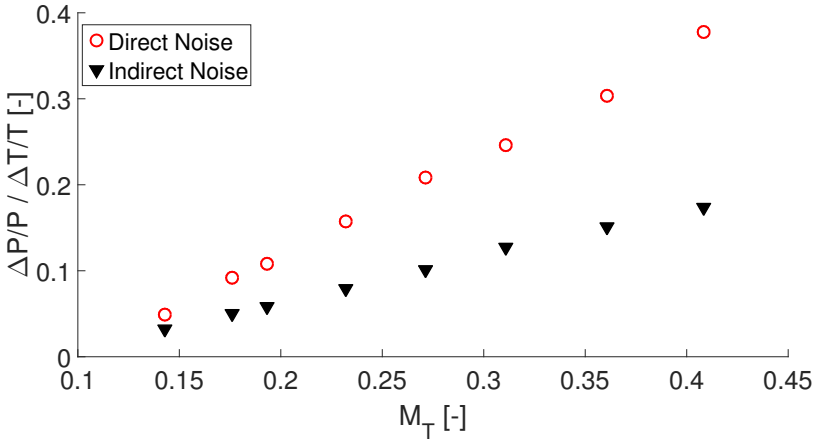

(b)

Figure 13: Absolute (a) and normalised (b) values of the peak of the acoustic oscillation of direct and indirect noise *vs.* estimated orifice Mach number in the long tube configuration.

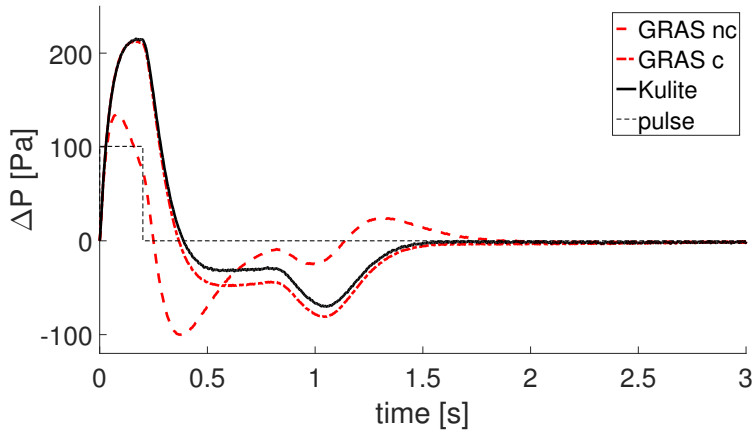

Figure 14: Ensemble-averaged pressure signal acquired 160 mm downstream of the heating module acquired by the Kulite pressure transducer (black solid line) and the G.R.A.S. microphone, before (red dashed line) and after (red dashed-dotted line) correction using its high-pass filter behaviour at low frequencies (Case C-3, long tube).

4.3.2. Comparison between the outputs of condenser microphones and piezoresistive pressure transducers

A note must be made regarding the usage of capacitive microphones in the present context. Figure 14 compares the pressure signal acquired by a G.R.A.S. microphone (red dashed line) and a Kulite pressure transducer (black solid line) for a bulk flow velocity of 1.24 m/s ($M_1 = 0.0036$) (case C-3). The signal of the G.R.A.S. microphone is inverted to account for the 180° polarity shift characteristic of a condenser microphone. The signal acquired with the G.R.A.S. transducer is both distorted and attenuated, and shows non-physical ringing caused by the high pass behaviour of the microphone. As expected, once this signal is filtered using the experimentally determined transfer function (red dashed-dotted line), it nearly matches both the shape and the amplitude of the signal obtained with the Kulite transducer. However, while the match for the direct noise is relatively good, the negative pressure peak and the indirect noise peak are still somewhat different.

Why are the present findings regarding the different types of microphone

relevant at all? The amplitude and shape of the pressure signal are essential for the understanding of the behaviour of the system. A distorted and/or attenuated output can lead to a misinterpretations of the results and a mismatching with the modelling. In prior experiments aimed to generate hot spots and thermoacoustic waves with unsteady electrical heating of thin wires and foils (DLR EWG [17, 18], Oxford EWG [23] and [40]), condenser microphones rather than pressure transducers were used, without mentioning if any correction was applied to the output of the microphones.

In [42] the issue of the microphone transfer function was brought up. However, the cut-on frequency obtained in [42] from numerical considerations is 12 Hz, 10 times larger than the cut-on frequency experimentally determined in this work and reported in the specifications of G.R.A.S. microphones [36]. Therefore, we suggest that in the future, all such low frequency measurements need to be verified for accuracy according to the calibration suggested here, or that piezo sensors be exclusively used for such low frequency experiments.

4.3.3. ***Short tube***

Figure 15 shows the pressure signal obtained 160 mm downstream of the heating module in the short tube configuration. A convective time $\tau_C \simeq 0.32$ s is estimated for the lowest flow velocity ($\bar{U}$=0.88 m/s), and $\tau_C \simeq 0.11$ s for the highest flow velocity ($\bar{U}$=2.52 m/s). As a result of this much smaller difference in characteristic time, direct and indirect noise have merged, and it is no longer possible to analyse the two separately. This merging results in an apparent change both in the shape and the amplitude of the direct and indirect acoustic oscillations. The direct noise appears as a positive increase in the pressure trace, as observed in Figure 12, while the indirect noise brings a negative contribution. However, when they superpose, both the positive and the negative peaks seem to decrease and the slope of the signal changes.

As shown in the case of the long tube (Fig. 13), the amplitude of the direct noise is nearly four times higher than that of the indirect noise, and has a dominant effect on the pressure signal. This may lead the indirect noise

contribution to be underestimated or neglected altogether. This can be clearly observed in Case C-8 ($\bar{U}$=2.52 m/s, short tube): the entropy spot reaches the nozzle 0.11 s after the beginning of the heating pulse, when the heating device is still active. The amplitude of the indirect noise peak seems smaller than in the $\bar{U}$=2.27 m/s case, whereas the direct noise is only slightly higher than in the $\bar{U}$=2.27 m/s case. However, as observed for the long tube configuration (Figures 11, 13) both the direct and indirect noise contributions increase nearly linearly with the Mach number. Thus, the apparent decrease in the indirect noise amplitude is an effect of the destructive interference of direct and indirect noise. This interaction can also be seen in the shape of the pressure oscillation: the sum of the negative oscillation with the positive direct noise peak effectively increases the decay rate of this positive oscillation.

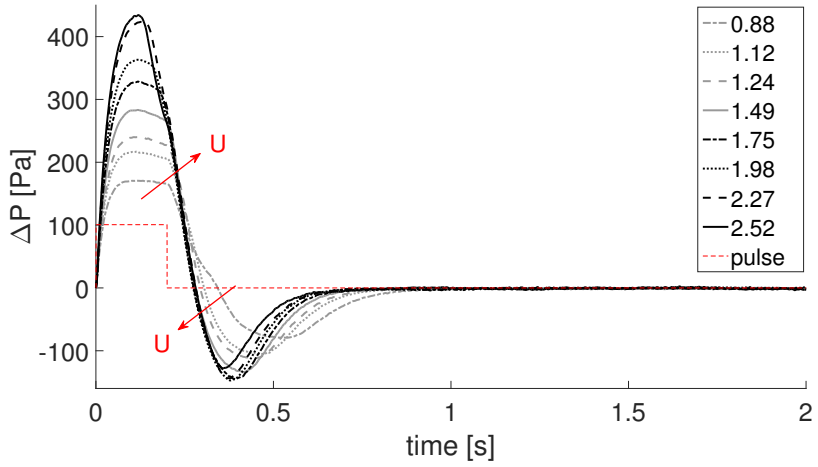

Figure 15: Ensemble-averaged pressure signal acquired by the Kulite transducer 160 mm downstream of the heating module. Legend indicates the magnitude of the bulk velocity (U) in m/s.

4.4. Case D: Accelerated flow (sonic)

Figures 16(a-b) show the pressure signals acquired in choked conditions with the 3 mm diameter orifice (black solid line) in the long and short tube configurations. From Figure 4 the pressure in the duct which corresponds to choked

conditions is around 1.9 $\times 10^5$ Pa. These results are compared with the corresponding results in the subsonic configuration (Case C-1, dark grey dashed line), and with the closed tube case (Case B, light grey dotted line). The reflection coefficient of a choked nozzle is comparable to that of a closed end: the velocity is imposed at the throat, which thus nearly behaves as a rigid wall (apart from a small mean flow effect).

The shape of the pressure signal in the choked configuration can be understood by comparing it with the acoustic oscillations in the subsonic and in the closed tube cases. Acoustic waves are created inside the tube when the heating device is active, and undergo repeated reflections at the two ends of the tube. Heat is exchanged from the heating device to the air via a convective mechanism, which is faster than the conductive mechanism in the closed tube condition, where the air is still. This results in a faster amplification of the acoustic energy in the system. When the heating device is no longer active, the acoustic energy starts to decay. The main difference relative to the closed tube appears due to the entropy waves: when the hot spots are accelerated through the nozzle, negative acoustic waves are generated, which are manifested as a change of the slope of the pressure decay, which becomes steeper. However, the pressure only becomes negative in the case of the long tube configuration. Indeed, the indirect noise generation starts when the acoustic energy of the direct noise has yet to dissipate, and the sum of the positive and negative cases results in the signal shape shown in Figures 16(a-b).

For the long tube configuration, the amplitude of the indirect noise can be estimated by isolating the negative pressure oscillation from the curve. The amplitude of this oscillation is $\Delta P_I \sim 290$ Pa. Comparing this value with the indirect noise peak for the same bulk velocity in subsonic conditions, the indirect noise in choked conditions is nearly 10 times higher in terms of absolute value and 6 times higher in terms of the normalised value than under subsonic conditions. With the short tube configuration, however, the amplitude of the indirect noise cannot be estimated in a straightforward way because the convective time of the entropy is too short and the indirect noise signal can not be

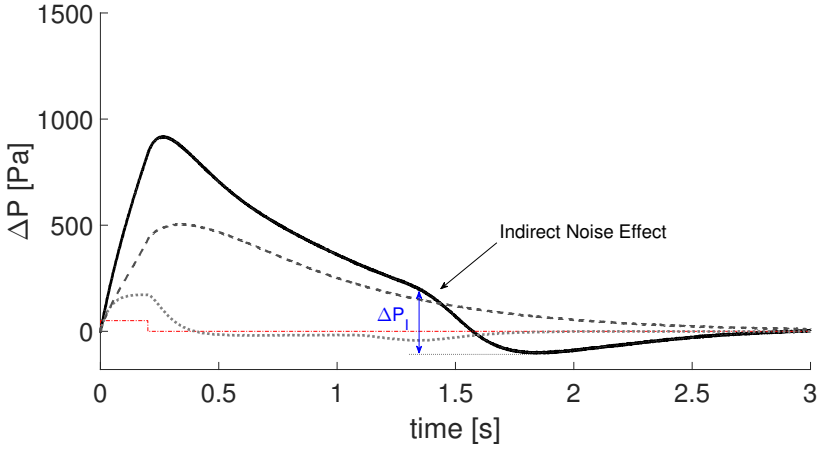

(a)

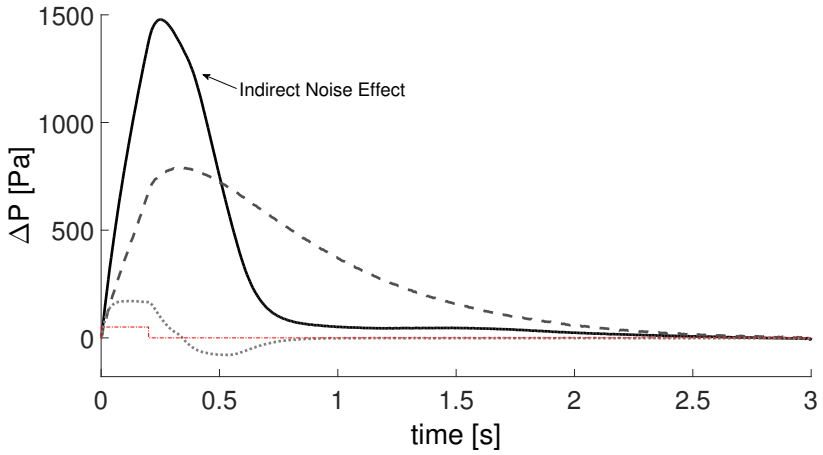

(b)

Figure 16: Averaged pressure signal acquired by the Kulite transducer 160 mm downstream of the heating module in the long (a) and short (b) tube. Black solid lines: choked tube; bulk flow velocity = 0.85 m/s (3 mm orifice); dark grey dashed lines: rigid wall (rigid wall with no flow); light grey dotted lines: subsonic flow, bulk flow velocity = 0.88 m/s (6.6 mm orifice).

extracted from the overall pressure trace, even if its influence as a change of the decay rate of the curve is clear.

5. Discussion on the results and further development

A detailed comparison between the experimental measurements and analytical models requires the full characterisation of the tube acoustics at the relevant low frequencies, both regarding the reflection coefficient of the orifice plate as well as the upstream end. Because of the ultra-low frequency range of interest, the calculation of the reflection coefficients is not straightforward. Whereas in general the orifice may be considered as a compact nozzle, potential losses need to be characterised for a fully quantitative comparison. Models for the transmissive and reflective properties of orifices can be found in the literature, but to the authors' knowledge, there is no information on their behaviour as a source of indirect noise.

The present experiments emphasise one of the major limitations of the current and previous studies: due to the physical behaviour of the wires, experiments can only be run in the ultra-low frequency range. This adds further complications to the understanding and modelling of the system due to the lack of experimental and analytical/numerical data in the infrasonic region. Moreover, the results are difficult to compare with a real physical situation. This suggests that it may be advantageous to consider alternative configurations capable of excitation/deexcitation frequencies closer to those of interest in real combustors, even if complications resulting from these alternatives may arise.

6. Conclusions

In this paper we have measured the backward propagating acoustic signals resulting from accelerating entropy spots generated by electrical heating, into outlet sections operated in subsonic and sonic conditions. The key result is the unambiguous identification of the contribution of direct and indirect noise in the overall noise. The acceleration of entropy spots is shown to generate

a significant acoustic signal. To the authors' knowledge, a clear identification and separation between direct and indirect noise for the reflected waves had not previously been demonstrated.

The indirect noise is isolated by choosing a convective time much longer than the electric pulse length. The indirect noise is then clearly identified by locating thermocouples in the orifice, which detect the arrival and acceleration of the hot spots: when the thermocouples start detecting an increase in air temperature, a pressure decrease is detected by the pressure transducers. This negative pressure excursion occurs earlier as the flow velocity is increased, due to a shorter convective time. We demonstrate that even for small flow accelerations (subsonic conditions), and low values of temperature fluctuations, indirect noise has a non-negligible contribution to the overall acoustic signal. However, direct noise is found to have a larger effect: when the heating device is active, a large pressure increase is detected by the pressure transducers. This pressure signal is caused by the air expanding due to the heat addition: no time lag is measurable between the heating pulse and this pressure pulse, which is therefore identified as direct noise. The peak amplitude of the direct noise is nearly four times higher than that of the indirect noise on average. From these results, it can be hypothesised that one of the reasons why the acoustic trace of entropy noise was not clearly detected in previous experiments is linked to the short convective time associated with the hot spots. In this experiment, a clear time separation between direct and indirect noise can be obtained only at low flow velocities (1-2 m/s) and long convective distances (1.4 m). With higher bulk flow velocities or shorter convective distances, the contribution of the indirect noise merges into the higher direct noise and can no longer be easily identified, even if it may affect the shape and amplitude of the pressure oscillation.

Another important result is the need to carefully account for the pressure transducer response at the very low frequencies typical of such rigs, which are limited by the cooling time of the wires. Condenser microphones behave as high pass filters, which significantly attenuate the pressure signal and lead to a phase shift at frequencies below about 10 Hz, and are unable to follow static

pressure increases or decreases. This generates non-physical ringings in the displayed output, which can lead to a misinterpretation of the results. Once the transfer functions of the microphones are taken into account, their outputs can be brought to a good agreement with piezoresistive transducers.

7. Acknowledgements

Francesca De Domenico is supported by the Honorary Vice-Chancellor's Award and a Qualcomm / DTA Studentship (University of Cambridge). Erwan Rolland is supported by an EPSRC DTA studentship (University of Cambridge). Experiments were partly funded by EPSRC grant EP/K02924X/1. Francesca De Domenico gratefully acknowledges Dr. Davor Dukic for his help with the electrical part of the experiment, Luca Magri for valuable advice and G.R.A.S. staff for their technical support.

References

[1] A. P. Dowling, S. Stow, Acoustic analysis of gas turbine combustors, Journal of Propulsion and Power 19 (5) (2003) 1–48. doi:10.2514/1.3538.

[2] http://cordis.europa.eu/search/simple_en, [Accessed 25 November 2016].

[3] http://cordis.europa.eu/result/rcn/52926_en.html, [Accessed 25 November 2016].

[4] http://cordis.europa.eu/project/rcn/104865_it.html, [Accessed 25 November 2016].

[5] J. W. S. Lord Rayleigh, The Theory of Sound, Macmillan, 1894.

[6] N. Kings, F. Bake, Indirect Combustion Noise : Noise Generation by Accelerated Vorticity in a Nozzle Flow, International Journal of spray and combustion dynamics 2 (2010) 253–266.

[7] L. Magri, J. O'Brien, M. Ihme, Compositional inhomogeneities as a source of indirect combustion noise, Journal of Fluid Mechanics 799 (2016) R4. doi:10.1017/jfm.2016.397.

[8] W. Polifke, C. O. Paschereit, K. Döbbeling, Constructive and Destructive Interference of Acoustic and Entropy Waves in a Premixed Combustor with a Choked Exit, Journal of Acoustics and Vibration 6 (3) (2001) 135–146.

[9] C. S. Goh, A. S. Morgans, The Influence of Entropy Waves on the Thermoacoustic Stability of a Model Combustor, Combustion Science and Technology (July 2015) (2012) 120816123400009. doi:10.1080/00102202.2012.715828.

[10] F. E. Marble, S. M. Candel, Acoustic Disturbance from Gas Non-Uniformities Convected Through a Nozzle, Journal of Sound and Vibration 55 (2) (1977) 225–243. doi:10.1016/0022-460X(77)90596-X.

[11] S. R. Stow, A. P. Dowling, T. P. Hynes, Reflection of Circumferential Modes in a Choked Nozzle, Journal of Fluid Mechanics 467 (2002) 1–25. doi:10.1017/S0022112002001428.

[12] I. Durán, S. Moreau, T. Poinsot, Analytical and Numerical Study of Combustion Noise Through a Subsonic Nozzle, AIAA Journal 51 (1) (2013) 42–52. doi:10.2514/1.J051528.

[13] A. P. Dowling, Y. Mahmoudi, Combustion Noise, Proceedings of the Combustion Institute 35 (1) (2015) 65–100. doi:10.1016/j.proci.2014.08.016.

[14] E. E. Zukoski, J. M. Auerbach, Experiments Concerning the Response of Supersonic Nozzles to Fluctuating Inlet Conditions, Journal of Engineering of Power 98(1) (1976) 60–64.

[15] M. S. Bohn, Noise Produced by the Interaction of Acoustic Waves and Entropy Waves with High Speed Nozzle Flows, Ph.D. thesis, California Insitute of Technology (1976).

[16] M. S. Bohn, Response of a Subsonic Nozzle to Acoustic and Entropy Disturbances, Journal of Sound and Vibration 52 (2) (1977) 283–297. doi:10.1016/0022-460X(77)90647-2.

[17] F. Bake, N. Kings, I. Roehle, Fundamental Mechanism of Entropy Noise in Aero-Engines: Experimental Investigation, Journal of Engineering for Gas Turbines and Power 130 (1) (2008) 011202. doi:10.1115/1.2749286.

[18] F. Bake, C. Richter, B. Mühlbauer, N. Kings, I. Röhle, F. Thiele, B. Noll, The Entropy Wave Generator (EWG): A reference case on entropy noise, Journal of Sound and Vibration 326 (3-5) (2009) 574–598. doi:10.1016/j.jsv.2009.05.018.

[19] B. Mühlbauer, B. Noll, M. Aigner, Numerical Investigation of the Fundamental Mechanism for Entropy Noise Generation in Aero-Engines, Acta Acustica united with Acustica 95 (3) (2009) 470–478. doi:10.3813/AAA.918171.

[20] M. S. Howe, Indirect Combustion Noise, Journal of Fluid Mechanics 659 (2010) 267–288. doi:10.1017/S0022112010002466.

[21] M. Leyko, S. Moreau, F. Nicoud, T. Poinsot, Numerical and analytical modelling of entropy noise in a supersonic nozzle with a shock, Journal of Sound and Vibration 330 (16) (2011) 3944–3958. doi:10.1016/j.jsv.2011.01.025.

[22] J. M. Lourier, A. Huber, B. Noll, M. Aigner, Numerical Analysis of Indirect Combustion Noise Generation Within a Subsonic Nozzle, AIAA Journal 52 (10) (2014) 1–13. doi:10.2514/1.J052755.

[23] M. I. Hake, Experimental Design to Determine the Effect of Temperature and Mach Number on Entropy Noise (MSc's Thesis), Tech. rep., Massachusetts Institute of Technology (2014).

[24] P. Gaetani, G. Persico, A. Spinelli, Entropy Wave Generator for Indirect Combustion Noise in a High-Pressure Turbine, in: Proceedings of the 11th

European Conference on Turbomachinery, Fluid Dynamics and Thermodynamics, 2015.

[25] K. Knobloch, L. Neuhaus, F. Bake, P. Gaetani, G. Persico, Experimental Assessment of Noise Generation and Transmission in a High-Pressure Transonic Turbine Stage, in: Proceedings of ASME Turbo Expo 2016: Turbomachinery Technical Conference and Exposition June 13-17, 2016, Seoul, South Korea, 2016, pp. 1–14.

[26] K. Knobloch, T. Werner, F. Bake, Noise Generation in Hot Nozzle Flow, in: Proceedings of the ASME Turbo Expo 2015: Turbine Technical Conference and Exposition GT2015-43702, 2015, pp. 1–14.

[27] S. Hochgreb, D. Dennis, I. Ayranci, W. Bainbridge, S. Cant, Forced and Self-Excited Instabilities from Lean Premixed, Liquid-Fuelled Aeroengine Injectors at High Pressures and Temperatures, in: Proceedings of the ASME Turbo Expo IGTI, June 3-7, 2013, San Antonio, Texas, USA, 2013, pp. GT2013—-95311. doi:10.1115/GT2013-95311.

[28] B. T. Chu, L. C. G. Kovasznay, Non-linear Interactions in a Viscous Heat-Conducting Compressible Gas, Journal of Fluid Mechanics 3 (1958) 494–514.

[29] L. Strobio Chen, S. Bomberg, W. Polifke, Propagation and generation of acoustic and entropy waves across a moving flame front, Combustion and Flame 166 (2016) 170–180. doi:10.1016/j.combustflame.2016.01.015. URL http://dx.doi.org/10.1016/j.combustflame.2016.01.015

[30] A. W. Bloy, The pressure waves produced by the convection of temperature disturbances in high subsonic nozzle flows, Journal of Fluid Mechanics 94 (03) (1979) 465. doi:10.1017/S0022112079001130.

[31] J. Li, D. Yang, C. Luzzato, A. Morgans, Open Source Combustion Instability Low Order Simulator (OSCILOS-Long), Tech. rep. (2015).

[32] H. H. Bruun, Hot Wire Anemometry: Principles and Signal Analysis, 1st Edition, Oxford University Press Inc., 1995.

[33] S. Carter, A. Ned, J. Chivers, A. Bemis, Selecting Piezoresistive vs . Piezoelectric Pressure Transducers. AN 102, Tech. rep. (Access date: February 2016).
URL http://www.kulite.com/docs/technical_papers/Piezoresistive_vs_Piezoelectric.pdf

[34] T. Nielsen, Precision Microphone for Measurements and Sound Reproduction, in: M. Gayford (Ed.), Microphone Engineering Handbook, Focal Press, 1994, pp. 62–139.

[35] A. J. Zuckerwar, Principles of Operation of Condenser Microphones, in: G. S. K. Wong, T. F. W. Embleton (Eds.), AIP handbook of condenser microphones, AIP press, 1995, Ch. 2, pp. 37–69.

[36] http://www.gras.dk/26ac.html, [Accessed 25 November 2016].

[37] H. Bodn, Influence of errors on the two-microphone method for measuring acoustic properties in ducts, The Journal of the Acoustical Society of America 79 (2) (1986) 541. doi:10.1121/1.393542.

[38] L. Trilling, On Thermally Induced Sound Fields, The Journal of the Acoustic Society of America 27 (3) (1955) 425–431.

[39] M. A. Brown, S. W. Churchill, Experimental Measurements of Pressure Waves Generated by Impulsive Heating of a Surface, Aiche Journal 41 (2) (1995) 205–213.

[40] I. Hwang, Y. Kim, Measurement of Thermo-Acoustic Waves Induced by Rapid Heating of Nickel Sheet in Open and Confined Spaces, International Journal of Heat and Mass Transfer 49 (3-4) (2006) 575–581. doi:10.1016/j.ijheatmasstransfer.2005.08.025.

[41] B. Farouk, Y. Lin, Z. Lei, Acoustic Wave Induced Flows and Heat Transfer in Gases and Supercritical Fluid, in: Y. Cho, G. Greene (Eds.), Advances in Heat Transfer (Vol.42), Elsevier, 2010, pp. 1–136.

[42] C. Becerril, S. Moreau, M. Bauerheim, L. Gicquel, T. Poinsot, Numerical investigation of Combustion Noise The Entropy Wave Generator, in: 22nd AIAA/CEAS Aeroacoustics Conference, 2016, pp. 1–18.